

# Modulation of Inflammation and Regeneration in the Intervertebral Disc Using Enhanced Cell-Penetrating Peptides for MicroRNA Delivery

Marcos N. Barcellona, Tara Ní Néill, Fergal J. O'Brien, James E. Dixon, Caroline M. Curtin, and Conor T. Buckley\*

Back pain is a global epidemiological and socioeconomic problem affecting up to 80% of people at some stage during their life and is often due to degeneration of the intervertebral disc (IVD). Therapies aimed at restoring the intradiscal space have predominantly focused on delivery of biomaterials, cells, or growth factors, among others, with variable degrees of success. While viral gene delivery strategies have emerged as promising therapeutic options in recent years, these approaches often have off-target effects and are associated with immunogenicity risks and other comorbidities. Consequently, nonviral methods have gained traction as potential avenues for gene delivery. Herein, enhanced cell-penetrating peptide (CPP) systems are used to deliver microRNAs in an *in vitro* and *ex vivo* model of disc degeneration. The data suggest that nanoparticle complexation of CPPs with (miR-221-inhibitor + miR-149-mimic) promotes protective effects in nucleus pulposus cells challenged with inflammatory cytokines TNF- $\alpha$  and IL-1 $\beta$ . Specifically, increases in matrix deposition, significant decreases in the secretion of an array of inflammatory cytokines, and decreased expression of matrix degradation enzymes MMP13 and ADAMTS5 are observed. These miR-CPP nanocomplexes can be further employed for targeting of the pericellular matrix space through homing, thus providing a promising approach for therapies of the intradiscal space.


## 1. Introduction

Intervertebral disc degeneration (IDD) is a complex condition affecting millions of people worldwide.<sup>[1,2]</sup> Although its origins remain to be fully elucidated, there exists a well-catalogued range of associated complications including changes in matrix composition, associated loss of tissue biomechanics, and altered levels of inflammatory cytokine secretion.<sup>[3–6]</sup> A variety of therapies have been developed to address IDD with variable degrees of efficacy, including biomaterials approaches,<sup>[7–11]</sup> cell therapies,<sup>[12–14]</sup> and soluble factor delivery.<sup>[15–17]</sup> MicroRNAs, small noncoding regulatory RNAs, have recently emerged as a promising class of nucleic acids for gene therapy applications, gaining traction due to their benefits in terms of transfection efficiency and high mechanistic specificity which allows for reduced off-target effects.<sup>[18–22]</sup>

Recent studies have discussed the modulatory effects of microRNAs on musculoskeletal tissue pathology, matrix

M. N. Barcellona, T. Ní Néill, F. J. O'Brien, C. M. Curtin, C. T. Buckley  
Trinity Centre for Biomedical Engineering (TCBE), Trinity Biomedical Sciences Institute (TBSI)  
Trinity College Dublin, the University of Dublin  
152-160 Pearse Street, Dublin D02 R590, Ireland  
E-mail: conor.buckley@tcd.ie

M. N. Barcellona, T. Ní Néill, F. J. O'Brien, C. M. Curtin, C. T. Buckley  
Advanced Materials and Bioengineering Research (AMBER) Centre  
Royal College of Surgeons in Ireland (RCSI) and  
Trinity College Dublin (TCD)  
Dublin D02 PN40, Ireland

 The ORCID identification number(s) for the author(s) of this article can be found under <https://doi.org/10.1002/anbr.202300112>.

© 2024 The Authors. Advanced NanoBiomed Research published by Wiley-VCH GmbH. This is an open access article under the terms of the Creative Commons Attribution License, which permits use, distribution and reproduction in any medium, provided the original work is properly cited.

DOI: 10.1002/anbr.202300112

F. J. O'Brien, C. M. Curtin, C. T. Buckley  
Tissue Engineering Research Group, Department of Anatomy and Regenerative Medicine  
Royal College of Surgeons in Ireland  
123 St. Stephen's Green, Dublin D02 YN77, Ireland

J. E. Dixon  
Regenerative Medicine & Cellular Therapies  
The University of Nottingham Biodiscovery Institute (BDI)  
School of Pharmacy  
University of Nottingham  
Nottingham NG7 2RD, UK

J. E. Dixon  
NIHR Nottingham Biomedical Research Centre  
University of Nottingham  
Nottingham NG7 2UH, UK

composition and degradation rates, and modulation of the inflammatory response.<sup>[19,23]</sup> Of particular interest were miR-149-5p-mimic and miR-221-3p-inhibitor, which have been suggested to have anti-inflammatory and proregenerative effects, respectively.<sup>[24–27]</sup> miR-149-mimic has been suggested to play a role in the pathophysiology of IDD by modulating inflammatory cytokine expression levels. Specifically, Qin et al. observed that following cell stimulation with lipopolysaccharide (LPS) and subsequent miR delivery, a downregulation in expression of TNF- $\alpha$  and IL-1 could be quantified.<sup>[27]</sup> Expression of such cytokines, namely, IL-1 $\beta$  and TNF- $\alpha$ , have been widely investigated in relation to degenerative disc disease (DDD), as these have been linked to increased incidence of intervertebral disc (IVD) herniation, decreased matrix synthesis,<sup>[28,29]</sup> and changes in nerve sensitivity,<sup>[30]</sup> among others. miR-221-inhibitor has been proposed to support matrix deposition rates in mesenchymal stem cell and chondrocyte cultures, with studies observing increased deposition of type II collagen, aggrecan, and expression of SOX9 to levels similar to those observed with TGF- $\beta$  treatment.<sup>[25,26]</sup>

The success of nucleic acid delivery depends on parameters such as cargo uptake and internalization, endosomal escape, and bioavailability,<sup>[31–33]</sup> all of which are correlated to the method of delivery. Commonly employed approaches can generally be divided into two major categories: viral and nonviral vectors. Within this field of research, viral approaches most often employ vectors such as adenoviral vectors for their high delivery efficiency or retroviral vectors for the incorporation of nucleic acids into the host cell's genome but can present risks of immunogenicity and significant off target effects.<sup>[31,34]</sup> Alternatively, the use of nonviral vectors for nucleic acid delivery presents an enticing approach for microRNA therapies due to reduced intrinsic risks of immunogenicity and therefore higher translational potential. Many different approaches have been explored in the literature with a range of success, including standard vector-free methods such as lipofectamine-mediated transfections, electroporation, nonviral vector carriers such as micelles and liposomes, and synthetic nanoparticles, among others.<sup>[31,35,36]</sup> In this study, we sought to employ two cell-penetrating peptides (CPPs) which have been reported to have high efficiency in cargo delivery in musculoskeletal applications: amphipathic peptide RALA<sup>[37,38]</sup> and glycosaminoglycan (GAG)-binding enhanced transfection peptide FLR.<sup>[39–41]</sup> These are both synthetic peptides designed to improve transfection efficiency and have been independently demonstrated to be compatible with a range of nucleic acids, including miRNA, siRNA, and plasmid DNA.<sup>[37,38,40]</sup> FLR was of particular interest as this synthetic CPP was specifically designed with an FGF2 heparin-binding domain, thus promoting homing effects toward GAG-rich areas.<sup>[33,40]</sup>

In the current work, we combine a miR-149-5p-mimic and miR-221-3p-inhibitor with nonviral vectors to explore their modulatory potential on matrix deposition and inflammatory cytokine secretion using primary rat nucleus pulposus (NP) cells. In monolayer as well as microtissue cultures, we observed our dual-miR-coupled CPPs to promote increases in matrix deposition and downregulation of secreted inflammatory cytokines. FLR-miR nanocomplexes are also observed to home to the pericellular matrix (PCM) space with high efficiency. The combinatorial delivery of miR-vector nanoparticles presented here may

yield an effective tool for disease modification with high tissue penetration efficiency and PCM localization.

## 2. Results

### 2.1. RALA and FLR Promote Increased Internalization Efficiency without Compromising Cell Viability

RALA and FLR both exhibited similar degrees of internalization efficiency compared to the lipofectamine control, reaching values of nearly 90% immediately following transfection (Figure 1A,B). A plateau in miR internalization could be observed at the 10 ng  $\mu\text{L}^{-1}$  concentration, with the 25 ng  $\mu\text{L}^{-1}$  miR-vector only promoting increased extracellular nanoparticle aggregation (Figure 1A,B and Supplementary Figure 1). A miR concentration of 10 ng  $\mu\text{L}^{-1}$  was therefore used for the remainder of the studies unless otherwise noted. Following 24 h or 7 d of culture, significant intracellular miR signal could still be observed (Figure 1C, E). Both CPPs also exhibited significantly higher degrees of cell viability compared to lipofectamine controls (Figure 1C,D).

### 2.2. Transfections with miR-221-Inhibitor and miR-149-Mimic-Vector Complexes Promote Increased Matrix Deposition and Decreased Expression of Matrix Degradation Enzymes in Monolayer

Cells were stimulated with inflammatory cytokines in order to promote elevated levels of matrix degradation enzymes (Supplementary Figure 2). Following, cells were transfected with either single-vector-miR-221-inhibitor, vector-miR-149-mimic, or with a dual-vector-(miR-221-inhibitor + miR-149-mimic). It was observed that transfection with miR-221-inhibitor promoted a significant increase in aggrecan deposition with RALA, and a nonsignificant trend toward increased aggrecan deposition in both FLR and lipofectamine control after 3 days of culture (Figure 2A,C). Collagen type 2 deposition was likewise elevated with both RALA and lipofectamine, with nonsignificant increase being observed in the FLR condition (Figure 2B,C). No significant changes could be observed in terms of MMP13 and ADAMT5 expression (Figure 2D–F). When the dual-miR transfection approach was employed, RALA and lipofectamine both promoted significant increases in both aggrecan and collagen II deposition, with FLR once again showing nonsignificant trends toward increased matrix deposition compared to nontransfected (NT) controls (Figure 2G–I). RALA and FLR both promoted significant decreases in MMP13 expression compared to both the NT and lipofectamine controls. Lipofectamine promoted an increase in ADAMT5 expression, which was not observed with either the RALA or FLR conditions. FLR demonstrated the largest decrease in ADAMT5 expression of the tested vectors (Figure 2J–L).

### 2.3. Dual-miR Transfection Promotes Trends toward Increased Matrix Deposition and Decreased Matrix Degradation Enzyme Expression

We formed cell microaggregates following transfection in order to culture cells in more relevant microenvironments. The microaggregates were either digested in papain and used for

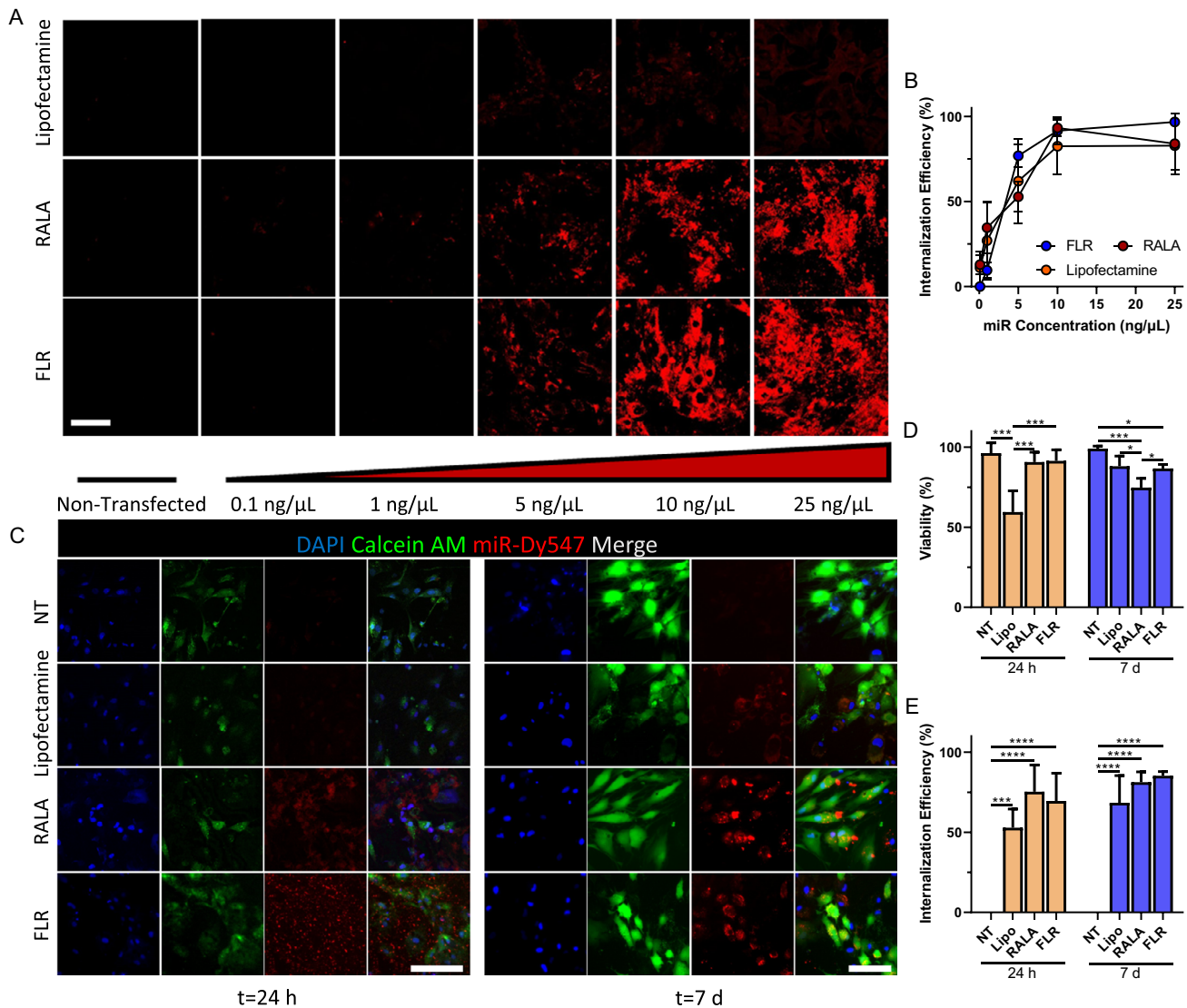


**Figure 1.** Vector-miR-Dy547 delivery: dosage and viability study. A) Dosage study using RALA, FLR, and lipofectamine complexed with increasing concentrations of miR-Dy547, compared against NT controls. Immunofluorescence images suggest efficient miR internalization as evidenced by homogeneous intracellular distribution and observable nuclear gap. B) Flow-cytometric quantification of miR-internalization efficiency following transfection. C–E) Characterization of intracellular miR retention and cell viability surveyed versus time using standard live/dead assay kits.  $N > 3$  biological replicates; each replicate composed of cells isolated from eight to ten discs pooled together. Statistical tests for all were one-way ANOVA's with Tukey's multiple comparison's test.  $*p < 0.05$ ,  $***p < 0.001$ , and  $****p < 0.0001$ . All scale bars are 100  $\mu\text{m}$ .

biochemical assays or wax-embedded and used for histology and immunolabeling. The biochemical data suggested nonsignificant trends toward increased deposition of GAGs and collagen in both RALA and FLR transfection conditions compared to lipofectamine-mediated transfections and NT controls. These trends were observable at both 3 (Figure 3A) and 14 d (Figure 3B) post-transfection. We observed significant degrees of cell death ( $\approx 45\%$ ) in lipofectamine-mediated transfections, while viability was similar for RALA and FLR and comparable to NT controls (Supplementary Figure 4). This can be further seen by the reduced pellet size and faint staining of the pellets in Figure 3A,B, where the medial-most section was taken for all pellets. Immunostaining for aggrecan and type 2 collagen

corroborated these trends, particularly at the 14-day timepoint (Supplementary Figure 4). Immunostaining for MMP13 and ADAMTS5 suggested a reduction in matrix degradation enzyme production in both RALA- and FLR-mediated transfections compared to both lipofectamine and NT controls (Figure 3C,D).

#### 2.4. Dual-(miR-221-Inhibitor + miR-149-Mimic) Transfection Promotes Decreased Expression of Inflammatory Cytokines

To survey the effect of dual-miR transfection on inflammation-associated cytokine secretion, we utilized an antibody microarray to detect cytokine presence from the media supernatant combined with the lysed cell microaggregate. Results suggested

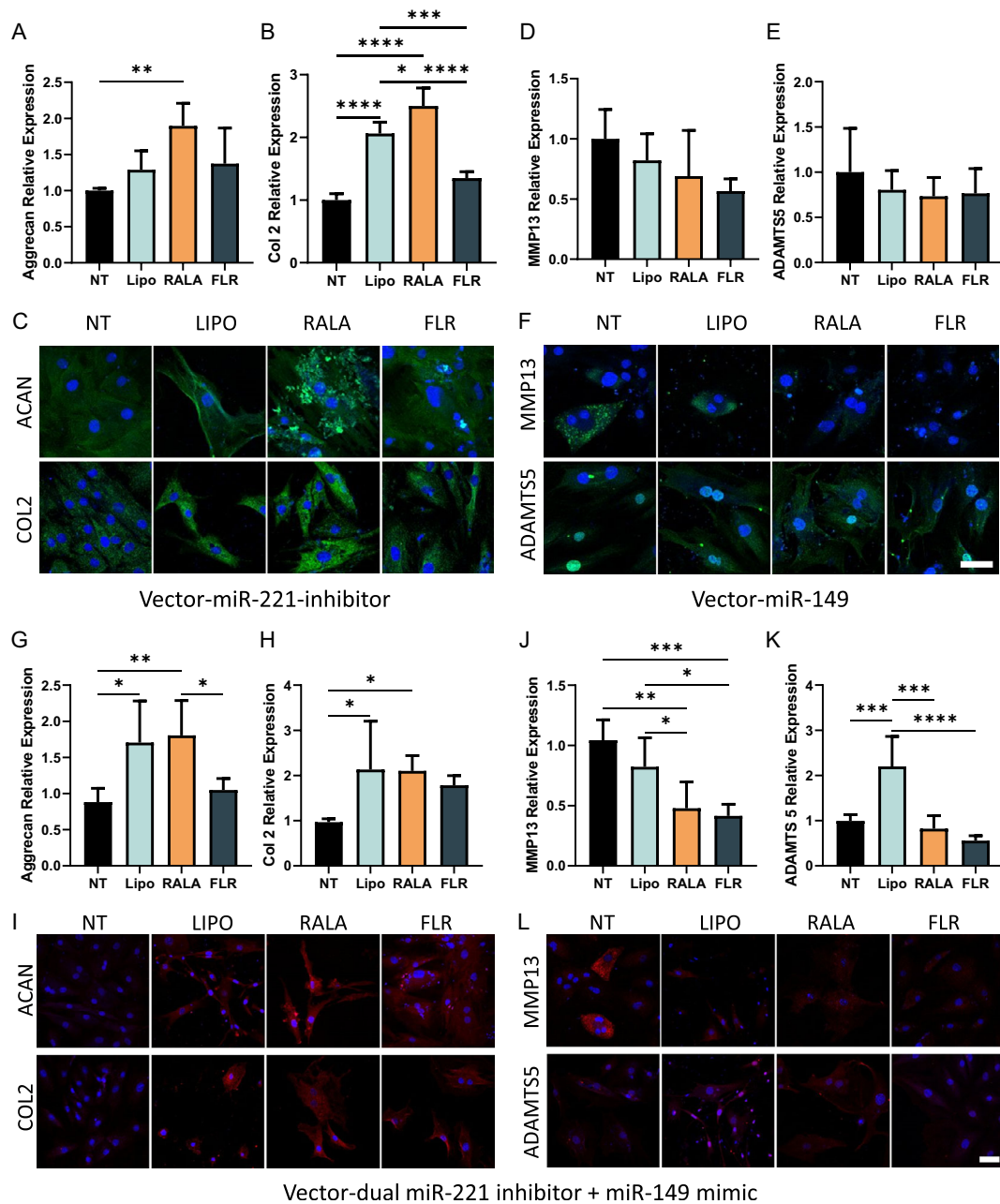


**Figure 2.** Transfection with individual and dual-miR complexes promotes increased matrix deposition and decreased expression of matrix degradation enzymes in monolayer. Cells were stimulated with inflammatory cytokines, and then followed by single-miR transfections with A–C) vector-miR-221-inhibitor and D–F) vector-miR-149-mimic; data suggest increases in deposition of aggrecan and collagen type II (A–C) as well as nonsignificant trends toward decreased expression of MMP13 and ADAMTS5 (D–F). Transfection with G–L) dual-miR-221-inhibitor + 149-mimic promotes similar degrees of aggrecan and collagen type II deposition (G–I), but stronger decreases in MMP13 and ADAMTS5 (J–L).  $N > 4$  biological replicates; each replicate composed of cells isolated from eight to ten discs pooled together. Statistics were one-way ANOVA's with Tukey's multiple comparison's test.  $*p < 0.05$ ,  $**p < 0.01$ ,  $***p < 0.001$ , and  $****p < 0.0001$ . Scale bars are 50  $\mu\text{m}$ .

decreased expression of key inflammatory cytokines including IFN- $\gamma$ , TNF- $\alpha$ , and IL-1 $\beta$ , among others (Figure 4). Downregulation could be observed as early as 3 d (Figure 4A), though the effect size increased by day 14, where significant decreases could be observed in expression of TNF- $\alpha$ , IL-1  $\alpha$ , IL-1 $\beta$ , IL-4, and IL-6 (Figure 4B) in both RALA and FLR groups compared to the NT condition as well as lipofectamine-mediated transfections.

### 2.5. FLR-Mediated Transfections Promote Pericellular Matrix Localization and Targeting

Homogeneous distribution of miR-Dy547 could be quantified for all transfection vectors at the 25 ng  $\mu\text{L}^{-1}$  condition, although only FLR-mediated transfections exhibited significant increases in signal intensity (Figure 5). For all conditions there was an



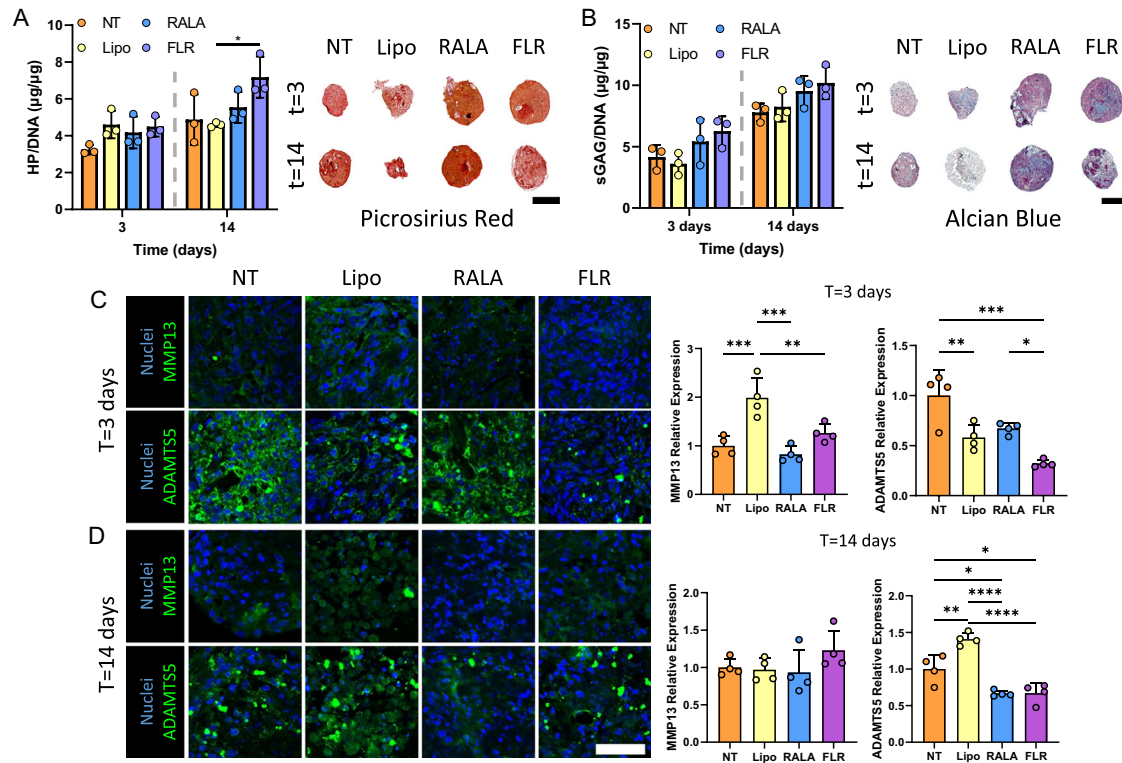


**Figure 3.** Transfection with dual-miR-coupled complexes promotes increased matrix deposition and decreased expression of matrix degradation enzymes in 3D microtissue culture. Biochemical and histological analysis for A) collagen and B) GAG demonstrated trends toward increased ECM deposition for RALA and FLR compared to NT. Scale bars are 200 µm. C–D) Immunofluorescence staining for matrix degradation proteins and associated semiquantitative analysis suggests decreases in MMP13 and ADAMTS5 expression, particularly with FLR-mediated transfections. Scale bars are 50 µm.  $N > 3$  biological replicates; each replicate composed of cells isolated from eight to ten discs pooled together. Statistics were one-way ANOVA's with Tukey's multiple comparison's test. \* $p < 0.05$ , \*\* $p < 0.01$ , \*\*\* $p < 0.001$ , and \*\*\*\* $p < 0.0001$ .

observed increase in signal intensity with increased miR concentration. For naked miR's, RALA, and lipofectamine mediated transfections, this signal remained diffuse and homogeneously distributed. In the FLR-mediated conditions, the GAG-homing effect could be observed as evidenced by increased signal intensity in the pericellular space. FLR-miR nanoparticles could be further observed to colocalize with COL VI-rich regions, suggesting an ability to home toward the PCM space (Figure 5).

### 2.6. FLR-Mediated Transfections Promote Highest Impact on Matrix Deposition Rates as Surveyed by Histological Outcomes

Delivery of dual-(miR-221-inhibitor + miR-149-mimic)-vector nanocomplexes suggested an increase in GAG content compared to the NT control, as evidenced by increased alcian blue staining (Figure 6A). RALA- and FLR-miR groups demonstrated a significant increase in SOX9 expression compared to the NT group. RALA and FLR promoted a decrease in MMP13 expression compared to NT, while lipofectamine-mediated transfections evidenced a subtle but significant increase in MMP13. RALA- and FLR-mediated transfections demonstrated significantly decreased ADAMTS5 expression compared to NT.

### 3. Discussion

MicroRNAs have become an attractive therapeutic tool due to their wide range of applications, as miRs have been documented in a number of biological processes from cell differentiation to regulation of the inflammatory response.<sup>[18,22,42,43]</sup> Specifically regarding the IVD, a significant number of miRs have now been reported<sup>[21]</sup> with observed roles in NP cell apoptosis,<sup>[44]</sup> ECM remodeling,<sup>[45,46]</sup> and inflammation,<sup>[27,47]</sup> among others. Dysregulation of miRNAs has been linked to disease progression,<sup>[21,48]</sup> and its artificial reregulation via exogenous delivery has been demonstrated to inhibit disease progression or even reverse specific degenerative target dysregulation in both in vitro and in vivo studies.<sup>[24,49–51]</sup>

A key shortcoming with miR delivery involves the targeting specificity of the approach. Here, we employed CPP-miR complexes for improved cell internalization efficiency and cargo delivery. The CPP-miR complexed nanoparticles are formed by simple electrostatic interactions between the negatively charged nucleic acids and positively charged CPPs, condensing into nanoparticles following their mixing at appropriate charge ratios. FLR and RALA CPPs were employed due to their reported abilities to efficiently deliver nucleic acids into cells derived from musculoskeletal tissues.<sup>[26,41]</sup> Furthermore, FLR was specifically

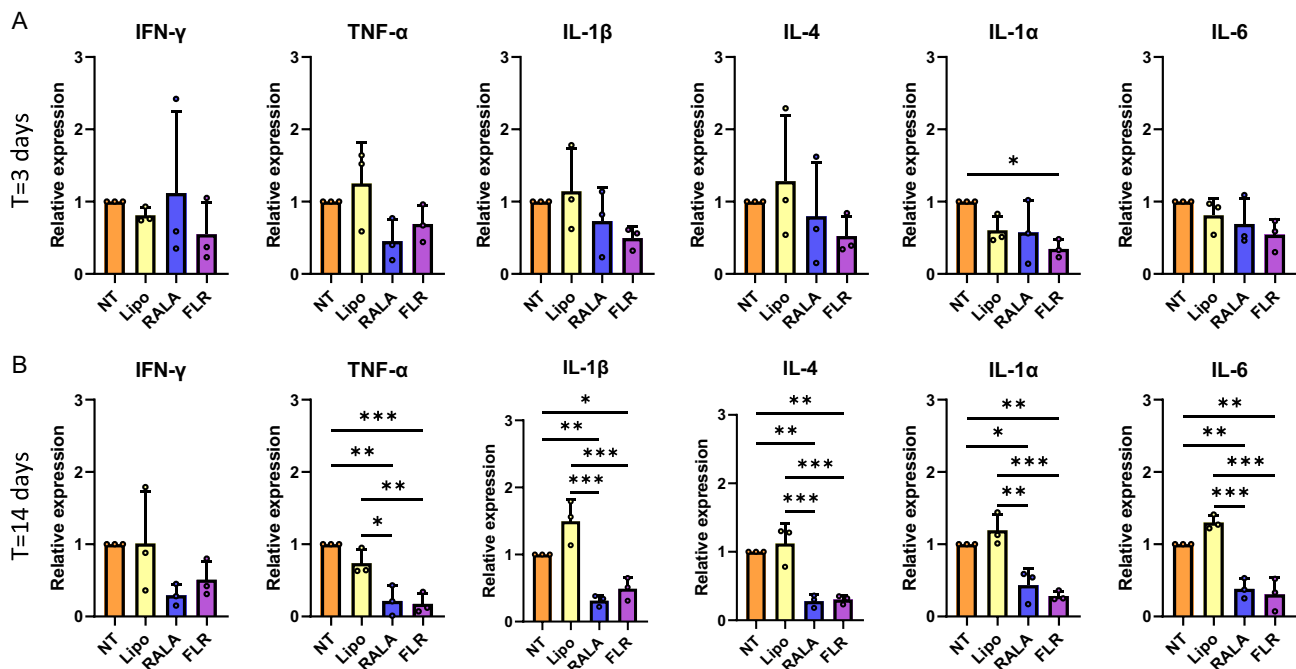


**Figure 4.** Antibody microarray panels for detection of inflammatory cytokine release suggest decreased cytokine levels in RALA and FLR mediated dual-miR transfections. RALA and FLR promote significant decreases in inflammatory cytokine release compared to both lipofectamine and NT conditions at 3 A) and 14 d B) post-transfection.  $N = 3$  biological replicates; each replicate composed of cells isolated from eight to ten discs pooled together. Statistics were one-way ANOVA's with Tukey's multiple comparison's test. \* $p < 0.05$ , \*\* $p < 0.01$ , \*\*\* $p < 0.001$ , and \*\*\*\* $p < 0.0001$ .

designed with a heparin-binding domain to promote homing toward GAG-rich areas.<sup>[33,40]</sup> This property presented an interesting avenue for investigation, as the NP is a naturally GAG-rich tissue. Indeed, the GAG-homing effects were best observed in the organ culture model, where there was strong signal condensation in the pericellular space when using the FLR-mediated nanoparticle delivery. We further observed signal colocalizing with areas positive for collagen type VI, a PCM protein known to interweave with GAGs.<sup>[52]</sup> In RALA and lipofectamine-mediated transfections, however, the miR-Dy547 signal remained more diffuse and uniformly distributed throughout the entire tissue section, without any clear localization pattern.

miR-221-inhibitor has previously been suggested to have strong prochondrogenic effects as evidenced by increased deposition of GAGs and Col2 following lipofectamine-mediated miR-221 inhibitor transfections in a cartilage regeneration model using bovine osteochondral biopsies.<sup>[26]</sup> miR-149-mimic, alternatively, has been suggested to play a role in the regulation of inflammatory cytokine production as well as matrix degradation enzyme expression.<sup>[27]</sup> Specifically, Qin et al. demonstrated that miR-149 delivery followed by LPS insult led to a protective effect in NP cells, promoting a significant decrease in TNF- $\alpha$  and IL-1 mRNA expression and repressing LPS-induced cell apoptosis.<sup>[27]</sup> In the current study, we observed increases in aggrecan and type 2 collagen deposition following dual miR transfection with both CPPs employed. A significant increase in SOX9 expression could be observed following dual-miR transfection with all vectors in the organ culture model, suggesting powerful prophenotypic effects. Additionally, significant decreases were observed in

expression of protein degradation enzymes MMP13 and ADAMTS5, as well as in the inflammatory cytokine release following dual miR transfections. Our data did not suggest synergistic functional outcomes in the dual miR-delivery approach when compared to the employment of individual miRs, but rather demonstrated an additive effect in functional outcomes. Further characterization is necessary to better understand the associated mechanisms such as pathway activation effects or competition between miRs.

While lipofectamine-mediated transfections promoted similar degrees of SOX9 expression, suggesting efficient carrier functions for miR delivery, it is important to note that this transfection method exhibited higher degrees of cell death than quantified with RALA- or FLR-mediated transfections. Furthermore, this technique demonstrated consistent trends toward increased expression of ADAMTS5 or MMP13, and increases in TNF- $\alpha$ , IL-1 $\beta$ , and IL-6, among others (full panel provided in Supplementary Figure 6). However, RALA- and FLR-mediated transfections did not appear to elicit the same proinflammatory effects.

In the organ culture model, we observed distinct spatial separation between GAG- and collagen-rich regions in the NP, with an increase in signal intensity often at a lateral aspect of the disc. This may be a consequence of the unilateral delivery of cABC and vector-miR nanoparticles into the intradiscal space for creation and treatment of tissue degeneration. Inclusion of mechanical stimulation in future experiments may simultaneously present a means to improve the physiological relevance of the bioreactor models while also promoting uniform dispersion and diffusion

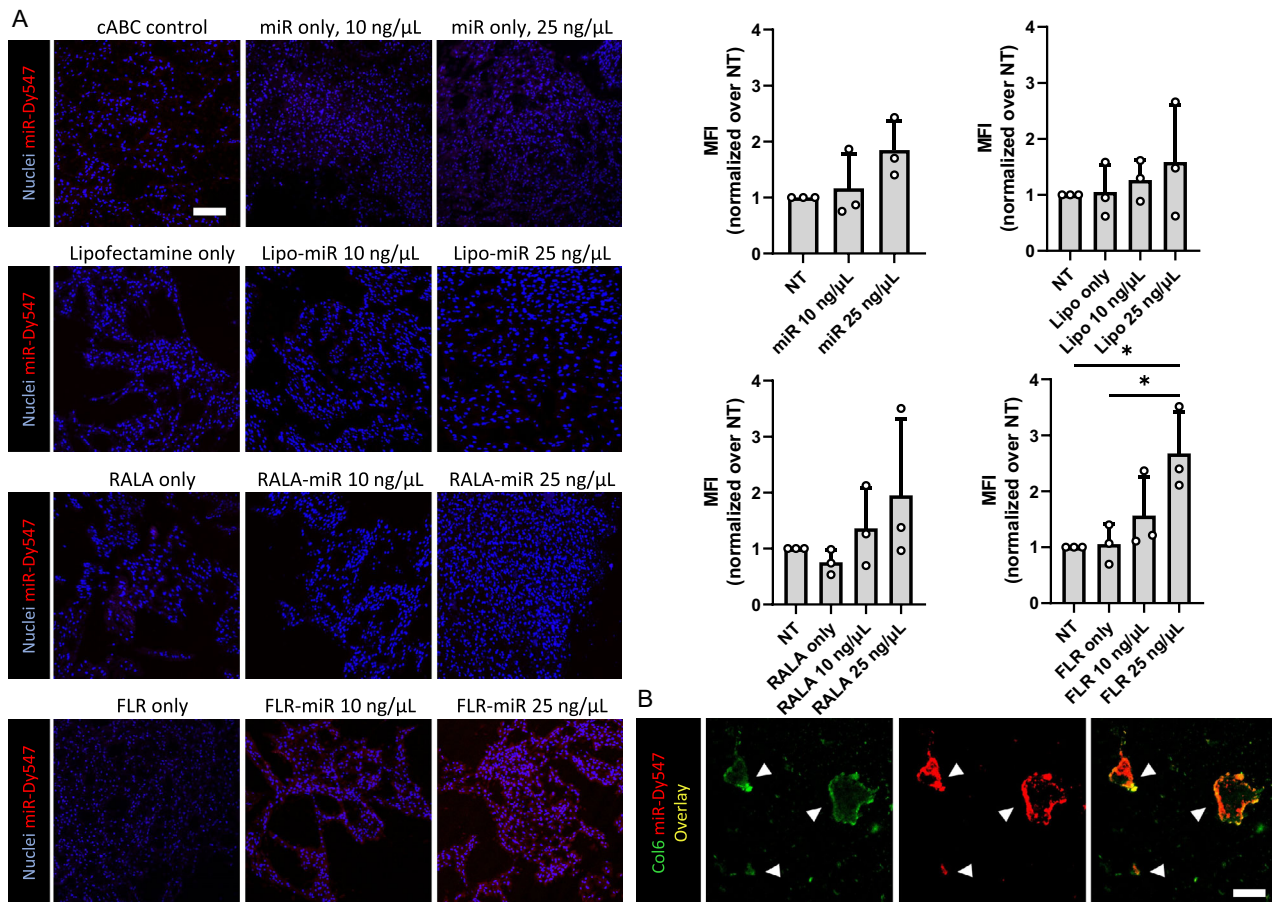


**Figure 5.** FLR promotes increased PCM localization of miR-vector nanoparticles. A) Delivery of naked miR, vector-only, or vector-miR nanoparticles at 10 and 25 ng mL<sup>-1</sup> demonstrate a dose-dependent increase in intradiscal signal intensity, with FLR demonstrating signal condensation in the PCM space and B) nanoparticle colocalization with COL6-rich regions. Scale bars are 100 μm. N = 3 biological replicates. Statistics were one-way ANOVA's with Tukey's multiple comparison's test. \**p* < 0.05.

of both cABC and consequent treatments intradiscally. Live/dead staining of the intradiscal space following 2 weeks of culture suggested no differences in viability between transfected and NT conditions (Supplementary Figure 7).

In this study, we utilized different dosages for monolayer cultures and organ culture models. Preliminary data suggested that dosages above 10 ng μL<sup>-1</sup> in monolayer resulted in significant nanoparticle aggregation and extracellular accumulation and even led to cytotoxicity. A dosage study in the organ culture model did not suggest increased cell death at the higher concentration of 25 ng μL<sup>-1</sup>, likely due to the increased complexity of the intradiscal space and high ECM content. This observation highlights the significant correlation between dosages and variables like cell type and physiological microenvironment, so adequate titration of miR concentrations is needed when modifying the delivery approach.

Another important consideration is the establishment of a microenvironment that allows for proper control of the relevant markers. In this instance, a proper inflammatory challenge was necessary in order to observe modulatory effects of functional miR transfections. While we observed an ability to downregulate

expression of matrix degradation enzymes in NP cells exposed to an inflammatory environment, it was observed that transfections with any of the studied vector-miR complexes without a pre-established challenge led to increased expression of MMP13 and ADAMTS5, likely due to cell damage from the transfection process itself (Supplementary Figure 3). A reduction in inflammatory cytokines and matrix degradation enzymes is thus observable due to elevated basal levels of these proteins following inflammatory insult. Nonetheless, further studies are still needed to better elucidate the mechanisms driving these functional changes. While rodent models do have associated limitations due to the presence of notochordal cells, smaller disc height, and higher cell density that is different to human, they serve as a valuable tool for assessing the feasibility of a technique before progressing to larger models. Therefore, we believe that our data retains its significance in advancing this approach, especially considering its early stage in research and the potential for clinical translation to human models.

Overall, our data demonstrates potential for employing CPPs to form nanoparticle complexes with the function modifying microRNAs miR-221-inhibitor and miR-149-mimic in order to



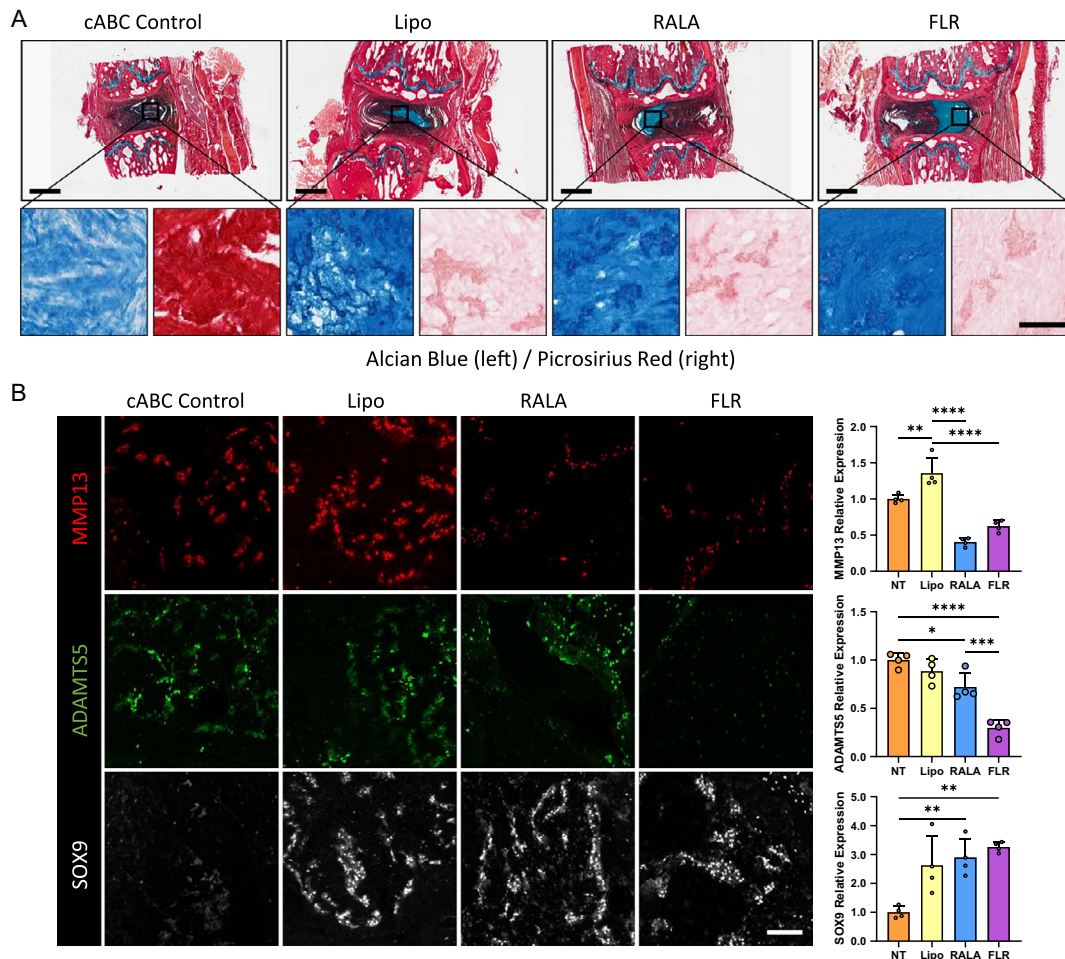


**Figure 6.** RALA- and FLR-mediated dual-miR transfections promote decreased expression of MMP13, ADAMTS5, and increased expression of SOX9. A) Rat disc sections following organ culture models of tissue degeneration and in situ transfections. Insets show alcian blue and picrosirius red staining. Scale bars for whole discs are 1 mm. Scale bars for insets are 100  $\mu$ m. B) Immunolabeling for MMP13, ADAMTS5, and SOX9, and associated quantification. Scale bars are 100  $\mu$ m.  $N \geq 3$  biological replicates. Statistics were one-way ANOVA's with Tukey's multiple comparison's test. \* $p < 0.05$ , \*\* $p < 0.01$ , \*\*\* $p < 0.001$ , and \*\*\*\* $p < 0.0001$ .

modulate extracellular matrix protein deposition and inflammatory cytokine secretion in in vitro models of disc degeneration. Together with the GAG-homing ability of the FLR peptide, this presents a promising avenue for the treatment of DDD.

#### 4. Experimental Section

**Primary Cell Isolation and Culture:** All procedures for this study were approved by the Animal Research Ethics Committee (AREC) of Trinity College Dublin and the Health Products Regulatory Authority (HPRA) in Ireland (Approval—AE19136/P149). NP tissue was obtained from caudal spines of Wistar rats (10–20 weeks), harvested under sterile conditions immediately post-euthanasia. Briefly, the skin was removed, and the tails were cleaned thoroughly with 70% ethanol and Povidone iodine solutions (Duggan Veterinary, Ireland). Following, a size 10 scalpel was used to make an incision along the transverse plane near a bounding endplate to expose the disc, and NP tissue was collected with needlepoint forceps. NP tissues from three tails (ten discs per tail) were pooled together, and cells were isolated following pre-established protocols.<sup>[53]</sup> Briefly, tissue was placed in a 50 mL conical tube and suspended in a combined solution

of collagenase II (100 U mL<sup>-1</sup>, Gibco, Life Technologies, USA) and pronase (10 U mL<sup>-1</sup>, Roche, Switzerland). A volume of 1 mL per disc was used. Digestions were allowed to proceed for 6 h at 37 °C on a rotator at  $\approx 10$  RPM. After primary cell isolation, cells were cultured at 37 °C and 5% O<sub>2</sub> in low glucose Dulbecco's modified eagle's medium (DMEM) + 10% FBS + 2% P/S (denoted XPAN media) and cultured up to passage 3.

**Vector-miR Nanoparticle Complexes:** Nanoparticles were formulated by the electrostatic interactions between anionic microRNA and cationic vectors at specific charge (N:P) ratios. The ratio of N:P is defined as the molar ratio of nitrogen atoms in the vectors (N) to phosphate groups in the microRNA (P). This ratio is a critical parameter in optimizing the electrostatic interactions for effective nanoparticle formation.<sup>[54]</sup> Specifically, combinations of miR-149-mimic (*Rattus norvegicus* rno-miR-149-5p sequence UCUGGCUCGGUGUCUUCACUCCCC), miR-221-inhibitor (*R. norvegicus* rno-miR-221-3p hairpin inhibitor sequence AGCUACAUUGUCU-GCUGGGUUUC), and miR-Dy547 (Horizon Discovery, UK), with vectors RALA (sequence: WEARLARALARARHLARALARALRACEA, N:P 10, GenScript, The Netherlands) or FLR (sequence: TYRSRKYTSWYVAALLK-RKLLKLLKLLKLLKRRRRRRR, N:P 5, Dixon Lab, University of Nottingham, UK) were prepared. Lipofectamine RNAiMAX (Thermo Fisher, USA) was used as a transfection control following manufacturer



recommendations. For all conditions, the vector carrier and miRs were combined within their appropriate parameters and complexes allowed to form for 30 min at room temperature (RT). All complexes were formed in serum-free OptiMEM (Gibco, ThermoFisher) and prepared fresh on the day of transfections.

**Cell Transfections:** Cells were plated in monolayer culture at a density of  $2\text{--}2.5 \times 10^4$  cells  $\text{cm}^{-2}$  in either 18-well chamber slides (Ibidi, Germany) for monolayer studies or  $8\text{--}10 \times 10^4$  cells  $\text{cm}^{-2}$  in wells of a 48 well plate for microaggregate studies and allowed to attach overnight in XPAN. Following, cells were washed with phosphate-buffered saline (PBS) and media was replaced with serum free DMEM (SF-DMEM) for 24 h. On the day of transfection, SF-DMEM was aspirated and the OptiMEM containing the formed vector-miR complexes was added to the wells and incubated at  $37^\circ\text{C}$  and  $5\% \text{O}_2$  for 6 h. The transfection media was then aspirated, fresh XPAN was added to each well, and cells were then incubated at  $37^\circ\text{C}$  and  $5\% \text{O}_2$  until the appropriate experimental time-point. To quantify internalization efficiency, complexes were formed with a fluorescently tagged nonfunctional miR-Dy-547. Internalization efficiency was visualized using a Leica SP8 scanning confocal microscope (Leica, Germany), and further quantified by trypsinizing the transfected cells, counterstaining with DAPI, and employing flow-cytometric analysis using an LSRFortessa Flow Cytometer 24 h post-transfection. Cell viability was determined using a live/dead kit (Invitrogen, USA) and imaged via confocal microscopy.

**Cytokine Challenge:** For studies focusing on transfection with functional-miRs, cells were challenged with proinflammatory cytokines prior to transfection to better mimic the typical in vivo microenvironment. Specifically, cells were plated in monolayer culture at  $2\text{--}2.5 \times 10^4$  cells  $\text{cm}^{-2}$  in either 18-well chamber slides, or in 48 well plates at a density of  $8\text{--}10 \times 10^4$  cells  $\text{cm}^{-2}$  and allowed to attach overnight in XPAN. Following, XPAN was aspirated and replaced with SF-DMEM, and cells were cultured for 24 h. Media was then replaced with SF-DMEM +  $50 \text{ ng mL}^{-1}$  TNF- $\alpha$  +  $10 \text{ ng mL}^{-1}$  IL-1 $\beta$  (PeproTech, USA)<sup>[29,55]</sup> and cells were cultured for an additional 24 h, at  $37^\circ\text{C}$  and  $5\% \text{O}_2$ . On the day of transfection, the cytokine-containing media was aspirated, cells were washed with PBS, and transfection reagents were applied as outlined above.

**Immunocytochemistry:** Cells were washed with  $1 \times$  PBS, and then fixed with 4% PFA for 12 min. Next, cells were permeabilized with 0.2% tritonX-100 for 20 min, rinsed with PBS, and then blocked with a solution of 5% BSA in PBS for 30 min. Immunolabeling was then performed overnight at  $4^\circ\text{C}$  using mouse-anti-MMP13 (Invitrogen MA514247), rabbit-anti-ADAMT55 (Invitrogen PA532142), rabbit-anti-aggrecan (Invitrogen MA532695), rabbit-anti-collagen II (Invitrogen PA599159), rabbit-anti-collagen VI (Invitrogen MA532412), or rabbit-anti-SOX9 (Invitrogen PA586301). Concentration-matched isotype controls were used for each antibody and in all experiments. Species-matched AlexaFluor (Invitrogen) secondary antibodies were applied, and cells were counterstained with Hoechst 33342 (Invitrogen). For cell viability, cells were stained with Calcein AM, and cell viability was calculated as the density of live (calcein positive) cells divided by the seeding cell density. Imaging was conducted on a Leica SP8 Scanning Confocal microscope. Relative expression data were collected using mean fluorescence intensity measurements of experimental conditions normalized over the controls, all obtained using  $N \geq 3$  regions of interest.

**Cell Microaggregate Formation and Culture:** Cells were plated in wells of a 48 well plate at a density of  $8\text{--}10 \times 10^4$  cells  $\text{cm}^{-2}$  and allowed to attach in XPAN overnight. Cells were then serum starved, exposed to a cytokine challenge, and transfected using the appropriate conditions for 6 h as outlined above. After transfection, cells were trypsinized and formed into microaggregates of  $3 \times 10^4$  cells by centrifugation for 5 min at 600 rcf. Microaggregates were maintained in culture in  $200 \mu\text{L}$  XPAN at  $5\% \text{O}_2$  and  $37^\circ\text{C}$ . Cultures were maintained for either 3 or 14 d, with full media exchange every 3 d.

**Biochemical Assays:** Sulfated GAGs were quantified using a Blyscan glycosaminoglycan assay (Biocolor Ltd., UK) following manufacturer recommendations. Briefly, samples were digested in 3.88 units/mL papain enzyme solution (papain in 100 mM sodium phosphate buffer/5 mM  $\text{Na}_2\text{EDTA}/10 \text{ mM}$  L-cysteine) for 18 h at  $60^\circ\text{C}$ , then incubated with the

DMMB reagent for 30 min, centrifuged to precipitate bound GAG, and resulting samples were combined with the dissociation agent and measured at 656 nm using a Synergy HT plate reader (BioTek Instruments). Collagen content was determined using a hydroxyproline assay. Briefly, papain-digested samples were combined with 37% HCl and incubated at  $110^\circ\text{C}$  for 18 h. Samples were then vented and dried at  $50^\circ\text{C}$  for 48 h, and the resulting contents were resuspended in ultrapure  $\text{H}_2\text{O}$ . Samples were then combined with 2.82% w/v chloramine-T and 0.05% w/v 4-(dimethylamino) benzaldehyde and measured at 570 nm. DNA content was measured using the Quant-iT PicoGreen dsDNA Reagent and Kit (Invitrogen) following manufacturer recommendations.

**Cytokine Secretion Assays:** Antibody microarrays (AssayGenie, Ireland) were employed for quantification of inflammation-associated markers in the supernatant following cytokine challenge and subsequent functional miR transfection. At experimental endpoints of 3 and 14 d, cell microaggregates were removed from culture and the supernatant was removed and processed following manufacturer recommendations. Briefly, patterned microarrays were blocked with blocking buffer for 30 min. Buffer was then removed, and media samples were incubated on the patterned microarrays for 2 h at RT. Membranes were then washed, biotinylated antibody cocktail was added to the microarrays, and arrays were cultured overnight at  $4^\circ\text{C}$ . The next day, the membranes were washed and incubated with a  $1 \times$  HRP-streptavidin solution for 2 h at RT. Following, the membranes were washed, and a supplied detection buffer mixture solution was added. Chemiluminescence detection was performed immediately after using a Bio Rad ChemiDoc Imaging System (Bio Rad, USA).

**Organ Culture:** Intact motion segments (comprised of vertebra-disc-vertebra units) were excised from the rat caudal spine immediately following euthanasia as previously described.<sup>[11]</sup> The tails were cleaned as described in Section 2.1, the skin was removed, and peripheral muscles were dissected to expose the intact disc. Motion segments were then placed in wells of a 6-well plate and cultured in XPAN at  $37^\circ\text{C}$  and  $5\% \text{O}_2$ .

To induce degeneration, a  $2 \mu\text{L}$  injection containing of bacterial chondroitinase (cABC, 0.0025 U) was delivered into the intradiscal space using a  $10 \mu\text{L}$  Hamilton syringe (Hamilton Company, USA) and a 30 G needle. Motion segments were then incubated for 1 week to allow mild degeneration to progress. Following, a  $2 \mu\text{L}$  injection containing  $25 \text{ ng mL}^{-1}$  of either vector-miR-Dy547 or vector-(miR-221-inhibitor + miR-149-mimic) was likewise delivered through a 30 G needle. Motion segments were cultured for the appropriate experimental times (3 d for fluorescently tagged nonfunctional miR colocalization studies, 2 weeks for functional miR delivery) in XPAN at  $37^\circ\text{C}$  and  $5\% \text{O}_2$ .<sup>[56–58]</sup>

**Histology and Immunohistochemistry:** At the experimental endpoints of cell microaggregate studies, the samples were fixed in 4% PFA for 20 min. All samples were then embedded in 3% w/v agarose, dehydrated in a graded series of ethanol (50–100%) and xylene, and paraffin wax embedded. For organ culture studies, motion segments were fixed in 4% PFA w/v for 48 h, and then decalcified in formic acid decalcification solution for an additional 4 d prior to dehydration in a graded series of ethanol, xylene, and wax embedded. Sections were obtained at a thickness of  $8 \mu\text{m}$  for microaggregates and  $12 \mu\text{m}$  for discs. Alcian blue and picosirius red staining were carried out as previously described.<sup>[59]</sup> For immunolabeling, sections were rehydrated by using a graded series of ethanol (100–30%) and water. Antigen retrieval was performed for disc sections by incubating in  $35 \text{ U mL}^{-1}$  pronase for 30 min at  $37^\circ\text{C}$ . Immunolabeling was then conducted as described above, using rabbit-anti-SOX9, mouse-anti-MMP13, and rabbit-anti-ADAMT55. Concentration-matched isotype controls were used for all antibodies, and species-matched AlexaFluor (Invitrogen) secondary antibodies were applied.

**CPP-miR Complex Homing of Pericellular Matrix:** To study the spatial distribution of vector-miR nanoparticles upon delivery, we created a defect by cABC delivery (0.0025 U in  $2 \mu\text{L}$ ) of ultrapure water into a rat caudal disc as described previously. We allowed degeneration to progress over 7 d, and then delivered  $2 \mu\text{L}$  of either miR-only, vector-only,  $10 \text{ ng mL}^{-1}$  vector-miR complex, or  $25 \text{ ng mL}^{-1}$  vector-miR complex to account for reduced bioavailability as a consequence of ECM presence. Injections were performed using a  $10 \mu\text{L}$  Hamilton syringe and 30 G

needle, and using a fluorescently tagged miR-Dy547 to observe miR-complex distribution.

To observe the GAG-homing effect of FLR, rat caudal discs were wax embedded as previously described, and then sectioned at a slice thickness of 12  $\mu\text{m}$ . Sections were rehydrated, and antigen retrieval was performed as described previously. Sections were blocked with PBS + 10% BSA for 30 min at RT, and stained with rabbit-anti-ColVI at RT for 2 h. Following, sections were washed 3 $\times$  and a solution containing 25 ng mL<sup>-1</sup> of miR-Dy547 nanoparticles was added and incubated overnight at 4 °C. A species-matched AlexaFluor was added to label col VI, and sections were then imaged using a Leica SP8 Scanning Confocal microscope.

**Statistics:** Statistical analysis was performed using GraphPad Prism (V 9.4.1) software. One-way ANOVAs with Tukey's multiple comparison tests were used to compare groups. All graphs are displayed as mean  $\pm$  standard deviation. Significance was accepted at  $p < 0.05$  for all tests.

## Supporting Information

Supporting Information is available from the Wiley Online Library or from the author.

## Acknowledgements

This project has received funding from the European Research Council (ERC) under the European Union's Horizon 2020 research and innovation program (grant agreement ERC-2019-CoG-864104; INTEGRATE).

## Conflict of Interest

The authors declare no conflict of interest.

## Data Availability Statement

The data that support the findings of this study are openly available in [Zenodo] at [10.5281/zenodo.7774959], reference number [7774959].

## Keywords

cell-penetrating peptides, intervertebral discs, miRNA

Received: October 12, 2023

Revised: March 9, 2024

Published online:

- [1] C. J. L. Murray, *JAMA* **2013**, 310, 591.  
 [2] D. Hoy, C. Bain, G. Williams, L. March, P. Brooks, F. Blyth, A. Woolf, T. Vos, R. Buchbinder, *Arthritis Rheumatol.* **2012**, 64, 2028.  
 [3] J. C. Iatridis, L. A. Setton, M. Weidenbaum, V. C. Mow, *J. Orthop. Res.* **1997**, 15, 318.  
 [4] P. J. Roughley, *Spine* **2004**, 29, 2691.  
 [5] M. A. Adams, P. J. Roughley, *Spine* **2006**, 31, 2151.  
 [6] J. P. G. Urban, S. Roberts, *Arthritis Res. Ther.* **2003**, 5, 120.  
 [7] R. D. Bowles, R. M. Williams, W. R. Zipfel, L. J. Bonassar, *Tissue Eng., Part A* **2010**, 16, 1339.  
 [8] H. Mizuno, A. K. Roy, C. A. Vacanti, K. Kojima, M. Ueda, L. J. Bonassar, *Spine* **2004**, 29, 1290.  
 [9] C. J. Panebianco, J. H. Meyers, J. Gansau, W. W. Hom, J. C. Iatridis, *Eur. Cell Mater.* **2020**, 40, 239.  
 [10] C. L. Gilchrist, E. M. Darling, J. Chen, L. A. Setton, S. Agarwal, *PLoS One* **2011**, 6, e27170.  
 [11] M. N. Barcellona, J. E. Speer, L. Jing, D. S. Patil, M. C. Gupta, J. M. Buchowski, L. A. Setton, *Acta Biomater.* **2021**, 131, 117.  
 [12] D. Sakai, G. B. J. Andersson, *Nat. Rev. Rheumatol.* **2015**, 11, 243.  
 [13] G. Vadala, G. Sowa, M. Hubert, L. G. Gilbertson, V. Denaro, J. D. Kang, *J. Tissue Eng. Regen. Med.* **2012**, 6, 348.  
 [14] S. Hiraishi, J. Schol, D. Sakai, T. Nukaga, I. Erickson, L. Silverman, K. Foley, M. Watanabe, *JOR Spine* **2018**, 1, e1013.  
 [15] A. Hu, R. Xing, L. Jiang, Z. Li, P. Liu, H. Wang, X. Li, J. Dong, *J. Biomed. Mater. Res., Part B* **2020**, 108, 2005.  
 [16] F. Zou, J. Jiang, F. Lu, X. Ma, X. Xia, L. Wang, H. Wang, *Mol. Med. Rep.* **2013**, 8, 118.  
 [17] C. Borrelli, C. T. Buckley, *Appl. Sci.* **2020**, 10, 9009.  
 [18] V. Baumann, J. Winkler, *Future Med. Chem.* **2014**, 6, 1967.  
 [19] P. Cazzanelli, K. Wuertz-Kozak, *Int. J. Mol. Sci.* **2020**, 21, 3601.  
 [20] L. F. R. Gebert, I. J. Macrae, *Nat. Rev. Mol. Cell Biol.* **2019**, 20, 21.  
 [21] C. Wang, L. Cui, Q. Gu, S. Guo, B. Zhu, X. Liu, Y. Li, X. Liu, D. Wang, S. Li, *Orthop. Surg.* **2022**, 14, 463.  
 [22] M. I. Almeida, R. M. Reis, G. A. Calin, *Mutat. Res., Fundam. Mol. Mech. Mutagen.* **2011**, 717, 1.  
 [23] P. Svoboda, *Front. Plant Sci.* **2020**, 11, 1237.  
 [24] Z. Wang, J. Hu, Y. Pan, Y. Shan, L. Jiang, X. Qi, L. Jia, *Inflammation* **2018**, 41, 959.  
 [25] A. Lolli, R. Narcisi, E. Lambertini, L. Penolazzi, M. Angelozzi, N. Kops, S. Gasparini, G. J. V. M. Van Osch, R. Piva, *Stem Cells* **2016**, 34, 1801.  
 [26] A. Lolli, K. Sivasubramaniyan, M. L. Vainieri, J. Oieni, N. Kops, A. Yayon, G. J. V. M. Van Osch, *J. Controlled Release* **2019**, 309, 220.  
 [27] C. Qin, Y. Lv, H. Zhao, B. Yang, P. Zhang, *Med. Sci. Monit.* **2019**, 25, 4892.  
 [28] C. Le Maitre, A. J. Freemont, J. Hoyland, *Arthritis Res Ther.* **2005**, 7, R732.  
 [29] J. Wang, D. Markova, D. G. Anderson, Z. Zheng, I. M. Shapiro, M. V. Risbud, *J. Biol. Chem.* **2011**, 286, 39738.  
 [30] C. Le Maitre, J. Hoyland, A. J. Freemont, *Arthritis Res. Ther.* **2007**, 9, R77.  
 [31] C. Du, H. Yan, J. Liang, A. Luo, L. Wang, J. Zhu, H. Xiong, Y. Chen, *Int. J. Nanomed.* **2017**, 12, 8599.  
 [32] L. A. Blokpoel Ferreras, S. Y. Chan, S. Vazquez Reina, J. E. Dixon, *ACS Appl. Nano Mater.* **2021**, 4, 167.  
 [33] H. M. Eltahir, J. Yang, K. M. Shakesheff, J. E. Dixon, *Acta Biomater.* **2016**, 41, 181.  
 [34] C. E. Thomas, A. Ehrhardt, M. A. Kay, *Nat. Rev. Genet.* **2003**, 4, 346.  
 [35] E. G. Tierney, G. P. Duffy, A. J. Hibbitts, S.-A. Cryan, F. J. O'Brien, *J. Controlled Release* **2012**, 158, 304.  
 [36] A. Bozkir, O. M. Saka, *Drug Delivery* **2004**, 11, 107.  
 [37] H. O. Mccarthy, J. Mccaffrey, C. M. Mccradden, A. Zholobenko, A. A. Ali, J. W. McBride, A. S. Massey, S. Pentlavalli, K.-H. Chen, G. Cole, S. P. Loughran, N. J. Dunne, R. F. Donnelly, V. L. Kett, T. Robson, *J. Controlled Release* **2014**, 189, 141.  
 [38] R. Bennett, A. Yakkundi, H. D. Mckeen, L. Mcclements, T. J. Mckeogh, C. M. Mccradden, K. Arthur, T. Robson, H. O. Mccarthy, *Nanomedicine* **2015**, 10, 2989.  
 [39] A. R. Jalal, J. E. Dixon, *Front. Bioeng. Biotechnol.* **2020**, 8, 849.  
 [40] J. E. Dixon, G. Osman, G. E. Morris, H. Markides, M. Rotherham, Z. Bayoussef, A. J. El Haj, C. Denning, K. M. Shakesheff, *PNAS* **2016**, 114, E291.  
 [41] H. A.-D. M. Abu-Awwad, L. Thiagarajan, J. E. Dixon, *Acta Biomater.* **2017**, 57, 225.  
 [42] M. L. Yeung, K.-T. Jeang, *Pharm. Res.* **2011**, 28, 3043.  
 [43] H. L. A. Janssen, H. W. Reesink, E. J. Lawitz, S. Zeuzem, M. Rodriguez-Torres, K. Patel, A. J. Van Der Meer, A. K. Patick, A. Chen, Y. Zhou, R. Persson, B. D. King, S. Kauppinen, A. A. Levin, M. R. Hodges, *N. Engl. J. Med.* **2013**, 368, 1685.

- [44] H.-Q. Wang, X.-D. Yu, Z.-H. Liu, X. Cheng, D. Samartzis, L.-T. Jia, S.-X. Wu, J. Huang, J. Chen, Z.-J. Luo, *J Pathol.* **2011**, 225, 232.
- [45] Z. Li, X. Yu, J. Shen, M. T.V. Chan, W. K. K. Wu, *Cell Proliferation* **2015**, 48, 271.
- [46] E. Tsirimonaki, C. Fedonidis, S. G. Pneumaticos, A. A. Tragas, I. Michalopoulos, D. Mangoura, D. Kletsas, *PLoS One* **2013**, 8, e82045.
- [47] Z. Chen, Y. Han, C. Deng, W. Chen, L. Jin, H. Chen, K. Wang, H. Shen, L. Qian, *J. Cell Phys.* **2019**, 234, 19977.
- [48] A. L. Kasinski, F. J. Slack, *Nat. Rev. Cancer* **2015**, 11, 849.
- [49] Y. Meng, R. Gao, J. Ma, J. Zhao, E. Xu, C. Wang, X. Zhou, *Sci. Rep.* **2017**, 7, 416.
- [50] N. Li, Y. Liu, Y. Miao, L. Zhao, H. Zhou, L. Jia, *IUBMB Life* **2016**, 68, 764.
- [51] S. Díaz-Prado, C. Cicione, E. Muiños-López, T. Hermida-Gómez, N. Oreiro, C. Fernández-López, F. J. Blanco, *BMC Musculoskeletal Disord.* **2012**, 13, 144.
- [52] E. R. Phillips, B. D. Haislup, N. Bertha, M. Lefchak, J. Sincavage, K. Prudnikova, B. Shallop, M. K. Mulcahey, M. S. Marcolongo, *J. Biomed. Mater. Res., Part A* **2019**, 107, 1977.
- [53] S. Basatvat, F. C. Bach, M. N. Barcellona, A. L. Binch, C. T. Buckley, B. Bueno, N. O. Chahine, A. Chee, L. B. Creemers, S. Dudli, B. Fearing, S. J. Ferguson, J. Gansau, B. Gantenbein, R. Gawri, J. D. Glaeser, S. Grad, J. Guerrero, L. Haglund, P. A. Hernandez, J. A. Hoyland, C. Huang, J. C. Iatridis, S. Illien-Junger, L. Jing, P. Kraus, L. T. Laagland, G. Lang, V. Leung, Z. Li, et al., *JOR Spine* **2023**, 6, e1238.
- [54] T. Gonzalez-Fernandez, B. N. Sathy, C. Hobbs, G. M. Cunniffe, H. O. Mccarthy, N. J. Dunne, V. Nicolosi, F. J. O'brien, D. J. Kelly, *Acta Biomater.* **2017**, 55, 226.
- [55] J. Wang, Y. Tian, K. L. E. Phillips, N. Chiverton, G. Haddock, R. A. Bunning, A. K. Cross, I. M. Shapiro, C. L. Le Maitre, M. V. Risbud, *Arthritis Rheumatol.* **2013**, 65, 832.
- [56] M. V. Risbud, M. W. Izzo, C. S. Adams, W. W. Arnold, A. S. Hillibrand, E. J. Vresilovic, A. R. Vaccaro, T. J. Albert, I. M. Shapiro, *Spine* **2003**, 28, 2652.
- [57] R. K. Ponnappan, D. Z. Markova, P. J. D. Antonio, H. B. Murray, A. R. Vaccaro, I. M. Shapiro, D. G. Anderson, T. J. Albert, M. V. Risbud, *Arthritis Res. Ther.* **2011**, 13, R171.
- [58] G. Lang, Y. Liu, J. Geries, Z. Zhou, D. Kubosch, N. Südkamp, R. G. Richards, M. Alini, S. Grad, Z. Li, *J. Tissue Eng. Regener. Med.* **2018**, 12, e2051.
- [59] C. Borrelli, C. T. Buckley, *Acta Biomater.* **2020**, 117, 142.